J. Fluid Mech. (1983), *vol.* 127, *pp.* 263–281
Printed in Great Britain

Numerical solutions for spin-up from rest in a cylinder

By JAE MIN HYUN,
Clarkson College of Technology, Department of Mechanical and Industrial Engineering, Potsdam, New York 13676

FRED LESLIE, WILLIAM W. FOWLIS
Space Science Laboratory, NASA Marshall Space Flight Center, Huntsville, Alabama 35812

AND ALEX WARN-VARNAS
Naval Ocean Research and Development Activity, Bay St Louis, Mississippi 39520

(Received 29 October 1981 and in revised form 8 September 1982)

Numerical solutions for the impulsively started spin-up from rest of a homogeneous fluid in a cylinder for small Ekman numbers are presented. The basic analytical theory for this spin-up flow is due to Wedemeyer (1964). Wedemeyer's solution shows that the interior flow is divided into two regions by a moving front which propagates radially inward across the cylinder. The fluid ahead of the front remains non-rotating, while the fluid behind the front is being spun up. Experimental observations have shown that Wedemeyer's model captures the essential dynamics of the azimuthal flow, but that it is not a quantitative model. Wedemeyer made several assumptions in formulating an Ekman compatibility condition, and inconsistencies exist between these assumptions and his solution. Later workers attempted to improve the analytical theory, but their work still included the same basic assumptions made by Wedemeyer.

No previous work has provided a comprehensive and accurate set of three-dimensional flow-field data for this spin-up problem. We chose to acquire such data using a numerical model based on the Navier–Stokes equations. This model was first checked against accurate laser-Doppler measurements of the azimuthal flow for spin-up from rest. New flow-field data over a range of Ekman numbers $9{\cdot}18 \times 10^{-6} \leqslant E \leqslant 9{\cdot}18 \times 10^{-4}$ are presented. Diagnostic studies, which reveal the various contributions to spin-up of the separate inviscid and viscous terms as functions of radius and time, are also presented. The plots of the viscous-diffusion term reveal the moving front, which is identified as a layer of enhanced local viscous activity. Immediately after the impulsive start, viscous diffusion is seen to be the major contributor to spin-up, then the nonlinear radial advection term takes over, and, finally, when spin-up is well progressed, the linear Coriolis force dominates. In the vicinity of the front, the inward radial flow is a maximum, and the vertical velocity is very small. Strong radial gradients of the vertical velocity are observed across the front and behind the front at the edge of the Ekman layer, and the azimuthal flow behind the front shows strong departures from solid-body rotation. These results enable us to fill in details of the flow not accurately given by Wedemeyer's model and its extensions.

1. Introduction

Spin-up is the general process of adjustment of an initially uniformly rotating fluid (angular velocity Ω_0) to an externally imposed change in the magnitude of the rotation rate of its container, $\Delta\Omega = \Omega - \Omega_0$, where Ω is the final angular velocity. A review by Benton & Clark (1974) is available for this subject.

In a definitive paper, Greenspan & Howard (1963) examined the spin-up of a homogeneous fluid occurring between two infinite rotating disks for an impulsive and small change in the rotation rates of the disks and hence for small values of the Rosby number $\epsilon \equiv \Delta\Omega/\Omega$. The rotation vector was taken as normal to the disks. They showed that the most important process controlling spin-up is the meridional circulation driven by Ekman layers on the endwalls. The interior fluid adjusts to the new rotation rate by the conservation of angular momentum and the concomitant stretching of vortex lines. This adjustment is substantially completed in the spin-up timescale $\tau \equiv E^{-\frac{1}{2}}\Omega^{-1}$, rather than in the viscous diffusion timescale $E^{-1}\Omega^{-1}$, where $E \equiv \nu/\Omega h^2$ is the Ekman number, ν is the kinematic viscosity of the fluid, and h is the depth of the fluid between the disks. The spin-up flows caused by larger changes in the rotation rate of the container, in which ϵ is no longer small, are complicated by nonlinear effects. However, the mechanism of the meridional circulation driven by Ekman boundary layers is still predominant, and the spin-up timescale is still given by τ (Greenspan 1968).

The basic analytical model for impulsive spin-up from rest of a homogeneous fluid in a cylinder is due to Wedemeyer (1964). Wedemeyer used an approximate method to formulate a single partial differential equation describing the azimuthal velocity in the interior. He made several assumptions when formulating an Ekman compatibility condition. Wedemeyer's solution shows that the interior flow is divided into two regions by a moving front, which propagates from the cylinder sidewall to the central axis. The fluid ahead of the front remains non-rotating, while the fluid behind the front is being spun up. Experimental observations have shown that Wedemeyer's model captures correctly the essential dynamics of the azimuthal flow but that it is not accurate in detail. When the assumptions are compared with the solution, several inconsistencies are found. Later workers have attempted to improve the analytical theory, but their work has all been based on the Wedemeyer model.

The objective of the work described in this paper was to develop a more accurate theoretical model of homogeneous spin-up from rest and to acquire more accurate data for both the azimuthal and meridional flows than had been accomplished previously. We decided to proceed using a numerical model and the model of Warn-Vernas *et al.* (1978) was chosen. This model was first checked by comparing its predictions against accurate experimental measurements of spin-up from rest using a rotating laser-Doppler velocimeter (LDV). For spin-up flows this procedure is much less tedious and can reveal more detail than an experimental measurement programme.

2. Previous work

2.1. *The Wedemeyer model*

Let (r, θ, z) denote cylindrical coordinates in an inertial frame of reference, and let (u, v, w) denote the corresponding velocity components. We take the mid-depth plane at $z = 0$ so that the fluid is confined in $0 \leqslant r \leqslant a$, $-\frac{1}{2}h \leqslant z \leqslant \frac{1}{2}h$, where a is the cylinder radius. Working from an order-of-magnitude analysis, Wedemeyer (1964) derived the

following equation for the azimuthal velocity v in the interior:

$$\frac{\partial v}{\partial t} + u\left(\frac{\partial v}{\partial r} + \frac{v}{r}\right) = \nu\left[\frac{\partial^2 v}{\partial r^2} + \frac{\partial}{\partial r}\left(\frac{v}{r}\right)\right]. \tag{1}$$

To reduce (1) to the one dependent variable v Wedemeyer derived an explicit functional relationship between u and v in the interior by considering the coupling between the interior flow and the Ekman-layer flow. To determine the Ekman suction effect, Wedemeyer used a linear approximation to the computations of Rogers & Lance (1960) for a fluid in steady solid-body rotation (Ω_I) above an infinite rotating disk (Ω). This procedure implies the following assumptions about the spin-up flow (Weidman 1976*a*):

(i) the boundary-layer flow is quasi-steady;

(ii) the finite geometry of the cylinder does not affect the boundary-layer flux;

(iii) the interior fluid is in solid-body rotation.

Assumption (i) is satisfactory in view of the large difference between the Ekman-layer formation timescale $O(\Omega^{-1})$ and τ. Assumptions (ii) and (iii) are somewhat severe and, as will be seen, lead to inconsistencies and inaccuracies in the Wedemeyer model.

Wedemeyer gave the relation between u and v as

$$u = E^{\frac{1}{2}}(v - r\Omega). \tag{2}$$

Upon substituting (2) into (1), we have

$$\frac{\partial V}{\partial T} + (V - R)\left(\frac{\partial V}{\partial R} + \frac{V}{R}\right) = A^{-2}E^{\frac{1}{2}}\left[\frac{\partial^2 V}{\partial R^2} + \frac{\partial}{\partial R}\left(\frac{V}{R}\right)\right], \tag{3}$$

where the non-dimensional quantities $R = r/a$, $V = v/a\Omega$, $T = t/\tau$ and $A = a/h$ have been introduced. Equation (3) is referred to as Wedemeyer's equation.

In the limit $A^{-2}E^{\frac{1}{2}} \ll 1$, when the right-hand side of (3) can be neglected, Wedemeyer found the analytic solution

$$V = 0 \quad (R \leqslant e^{-T}), \tag{4a}$$

$$V = \frac{R e^{2T} - R^{-1}}{e^{2T} - 1} \quad (R \geqslant e^{-T}). \tag{4b}$$

Equations (4*a*, *b*) clearly indicate that the interior flow is divided into two regions by a moving front located at $R = e^{-T}$, which propagates from the cylinder wall ($R = 1, T = 0$) to the central axis ($R = 0, T \to \infty$). Note that, although V is continuous across the front, $\partial V/\partial R$ is not. The angular velocity in the region ahead of the front ($R < e^{-T}$) remains zero. In the region behind the front ($R > e^{-T}$) the azimuthal velocity consists of a superposition of a time-dependent rigid rotation and a time-dependent potential vortex. Thus we have solid-body rotation (actually $V = 0$) ahead of the front, but we do not have solid-body rotation behind the front. This result is not consistent with assumption (iii).

Substituting (4) into (2) and using the continuity equation, the vertical velocity w in the interior is found as

$$w = 2E^{\frac{1}{2}}\Omega z \quad (R < e^{-T}), \tag{5a}$$

$$w = \frac{-2E^{\frac{1}{2}}\Omega z}{e^{2T} - 1} \quad (R > e^{-T}), \tag{5b}$$

demonstrating that the vertical velocity is linear in z and is a step function in r, with a discontinuity at the front $R = e^{-T}$. It follows immediately from (5) that the normal

velocity at the edge of the Ekman layer at the bottom disk, $\tilde{w}_\infty$, is given by

$$\tilde{w}_\infty = -E^{\frac{1}{2}}\Omega h \quad (R < e^{-T}), \tag{6a}$$

$$\tilde{w}_\infty = \frac{E^{\frac{1}{2}}\Omega h}{e^{2T}-1} \quad (R > e^{-T}). \tag{6b}$$

These equations show that there is uniform, constant suction of the fluid by the Ekman layer ahead of the front, and uniform time-dependent blowing behind the front. This result is not consistent with assumption (ii) of the model.

2.2. *Extensions of the Wedemeyer model*

Venezian (1969, 1970) returned to Wedemeyer's viscous equation, (3), and, by use of a stretched coordinate in the vicinity of the front, showed that the front is actually a moving layer of thickness $O(E^{\frac{1}{4}}h)$. He gave the following approximate solution for the azimuthal velocity in the neighbourhood of the front:

$$V = 4E^{\frac{1}{4}}(2\pi\eta)^{-\frac{1}{2}}[AR\exp(\beta^2)\operatorname{erfc}\beta]^{-1}, \tag{7}$$

where $\eta = e^{2T}-1$, $\beta^2 = A^2(R^2e^{2T}-1)^2/8E^{\frac{1}{2}}\eta$, and erfc is the complementary error function.

The effect of the viscous diffusion term was also examined by Watkins & Hussey (1973, 1977), who integrated numerically Wedemeyer's viscous equation, (3). Watkins & Hussey also made measurements of the azimuthal flow during spin-up from rest using a stationary LDV. They compared their numerical results with their measurements and found good agreement.

Watkins & Hussey compared their numerical results with Wedemeyer's inviscid solution, (4), and with Venezian's viscous solution, (7). They concluded that the Wedemeyer inviscid solution is valid in the limit of vanishing $A^{-2}E^{\frac{1}{2}}$, except near the front and at extremes of radial position ($R \approx 1$ or $R \approx 0$). Even for small values of $A^{-2}E^{\frac{1}{2}}$ ($\approx 0{\cdot}004$), the comparisons show that the Wedemeyer inviscid solution deviates considerably from the numerical solution in the neighbourhood of the front. For the same small values of $A^{-2}E^{\frac{1}{2}}$, Venezian's solution is shown to agree well with the numerical solution, not only in the neighbourhood of the front, where it is a substantial improvement over Wedemeyer's theory, but also over a wide range of T and R. However, as $A^{-2}E^{\frac{1}{2}}$ increases, Venezian's theory gives an increasingly poorer representation of the flow, and, for small R and large T, Venezian's solution blows up. Comparisons of Wedemeyer's and Venezian's results are given in figure 1.

Another extension of Wedemeyer's model was made by Weidman (1976*a*, *b*). Weidman used an accurate polynomial fit to the data of Rogers & Lance (1960) in formulating an Ekman compatibility condition for Wedemeyer's equation. He found intersecting characteristics near the front yielding a discontinuity in v itself rather than $\partial v/\partial r$. Thus Weidman demonstrated that this approach does not improve the Wedemeyer model.

2.3. *A numerical model*

Numerical simulations of spin-up flows have been reported by Kitchens (1979, 1980), who developed an axisymmetric code to solve the stream-function–vorticity form of the incompressible Navier–Stokes equations in cylindrical coordinates using a predictor–corrector multiple-iteration scheme. The grid-point distribution was optimized using coordinate transformations to resolve simultaneously details of both the interior and the endwall and sidewall boundary layers. To check his code, Kitchens made comparisons with the quasi-linear results of Warn-Varnas *et al.* (1978) and with

the experimental measurements of spin-up from rest of Watkins & Hussey (1977), and he obtained very good agreement.

Kitchens presented meridional stream-function plots of homogeneous spin-up from rest for times shortly after the impulsive start. He found and discussed inertial oscillations and reverse-flow regions close to the sidewall for early times and for small values of $A^{-2}E^{\frac{1}{2}}$. Kitchens also used his model to compute the Ekman-layer radial mass flux and he compared his results with the data of Rogers & Lance (1960). The agreement was not good, demonstrating the inaccuracy of the simple Ekman compatibility assumption. Kitchens derived a nonlinear Ekman compatibility condition. He found a monotonic relation, but he also found no unique relation that is valid for all A, E, R and T. Kitchens' papers do not contain flow-field data for intermediate and later times. He gave no data on the moving front.

2.4. *Discussion of the previous work*

The Wedemeyer model and its extensions have revealed much about the dynamics of spin-up from rest, but none of these models can be considered as a quantitative model that is accurate throughout the spin-up process. The inconsistencies in the Wedemeyer model are related to the assumptions made in formulating the Ekman compatibility condition (2). The extensions to the Wedemeyer model do not remove these inconsistencies, since they are based on the same assumptions.

The deficiencies of the Wedemeyer model and its extensions have been discussed by Benton (1979). In particular, Benton pointed to the implausibility of the vorticity dynamics. Wedemeyer's solution, (4), reveals that the axial vorticity $\zeta(\equiv r^{-1}\partial(rv)/\partial r)$ is zero ahead of the front and is non-zero, uniform and greater than 2Ω behind the front. Thus, although the interior azimuthal flow is less than the speed of the solid boundary, suggesting the use of the von Kármán branch ($\Omega_I < \Omega$) of the Rogers & Lance data, the vorticity criterion suggests the use of the Bödewadt branch ($\Omega_I > \Omega$). Benton concluded that the Wedemeyer model cannot be trusted in detail and that the use of a simple Ekman suction formula to parameterize the entire endwall boundary layer is inadequate. He pointed to the need to develop a nonlinear Ekman compatibility condition for boundary layers underlying interior flows with strong radial variations. This was attempted by Kitchens (1979) (see §2.3).

3. The numerical model and its verification

The numerical solutions for impulsive spin-up from rest were carried out using the code of Warn-Varnas *et al.* (1978). The axisymmetric incompressible Navier–Stokes equations in cylindrical coordinates (r, θ, z) rotating with the angular velocity Ω for the respective relative velocity components (u, v', w) are

$$\frac{\partial u}{\partial t} = -\frac{1}{r}\frac{\partial}{\partial r}(ruu) - \frac{\partial}{\partial z}(uw) + \frac{v'^2}{r} + 2\Omega v' - \frac{1}{\rho}\frac{\partial p}{\partial r} + \nu\left[\frac{\partial}{\partial r}\frac{1}{r}\frac{\partial}{\partial r}(ru) + \frac{\partial^2 u}{\partial z^2}\right], \tag{8}$$

$$\frac{\partial v'}{\partial t} = -\frac{1}{r}\frac{\partial}{\partial r}(ruv') - \frac{\partial}{\partial z}(v'w) - \frac{v'u}{r} - 2\Omega u + \nu\left[\frac{\partial}{\partial r}\frac{1}{r}\frac{\partial}{\partial r}(rv') + \frac{\partial^2 v'}{\partial z^2}\right], \tag{9}$$

$$\frac{\partial w}{\partial t} = -\frac{1}{r}\frac{\partial}{\partial r}(ruw) - \frac{\partial}{\partial z}(ww) - \frac{1}{\rho}\frac{\partial p}{\partial z} + \nu\left[\frac{1}{r}\frac{\partial}{\partial r}\left(r\frac{\partial w}{\partial r}\right) + \frac{\partial^2 w}{\partial z^2}\right]. \tag{10}$$

Here p denotes the pressure (which includes the hydrostatic pressure and the centrifugal potential) and ρ the density. Note that the azimuthal velocity v referred

to in the inertial frame is related to v' through

$$v = v' + r\Omega. \tag{11}$$

The continuity equation is

$$\frac{1}{r}\frac{\partial}{\partial r}(ru) + \frac{\partial w}{\partial z} = 0. \tag{12}$$

The initial conditions for the fluid are

$$u = w = 0, \quad v' = -r\Omega \quad (t = 0). \tag{13}$$

The boundary conditions on the cylinder wall and on the bottom and the top disks are

$$u = v' = w = 0 \quad (r = a), \tag{14a}$$

$$u = v' = w = 0 \quad (z = \pm \tfrac{1}{2}h). \tag{14b}$$

To satisfy numerical stability requirements, the boundary conditions at the central axis are applied at a small, but finite, radius ($r = r_i$):

$$u = 0, \quad v' = -r_i\Omega, \quad \frac{\partial w}{\partial r} = 0 \quad (r = r_i). \tag{15}$$

3.1. *Numerical simulation technique*

Equations (8)–(12) and the initial and boundary conditions were finite-differenced on a staggered mesh. To resolve the thin Ekman boundary layers (of thickness $O(E^{\frac{1}{2}}h)$) near the endwalls the grid was stretched in the z-direction. This stretching was accomplished by the use of the function $\xi = \tanh(z/z_b)$, where z_b is a parameter that controls the stretching. The grid spacing was uniform in the r-direction in order to resolve better the moving front (of thickness $O(E^{\frac{1}{4}}h)$) in the interior. Actual computations were performed on a 42-by-42 grid in the full domain. The dependent variables were distributed over the staggered grid (see figure 2 of Warn-Varnas *et al.* 1978). The pressure was found from the Poisson equation obtained by taking the divergence of (8) and (10). This equation is

$$\frac{\partial D}{\partial t} = -\nabla^2 p + C,$$

where C denotes the combined divergence of the advection and Coriolis terms in the u- and w-equations. D is the divergence ($\nabla \cdot \mathbf{u}$), which is small but, owing to machine round-off errors, not zero. This equation was solved by an ADI iterative approach. For further details on the numerical techniques, see Warn-Varnas *et al.* (1978).

3.2. *Verification of the numerical model*

The numerical model adopted has been verified previously for quasi-linear, homogeneous and stratified spin-up flows (see Warn-Varnas *et al.* 1978; Hyun, Fowlis & Warn-Vernas 1982). These verifications were made by checking the model predictions against accurate rotating LDV measurements. This method was used again in this study to verify the code for the strongly nonlinear problem of spin-up from rest.

The experimental apparatus consisted of a Plexiglas, cylindrical container (radius $a = 10{\cdot}15$ cm, height $h = 10{\cdot}05$ cm), mounted on a precision-rate turntable with its axis of symmetry maintained vertical and made coincident with the rotation axis. The container was filled with water, with kinematic viscosity $\nu = 9{\cdot}3 \times 10^{-3}$ cm^2 s^{-1}. Azimuthal-flow measurements were made with an LDV system, mounted on the

turntable. The optical arrangement of this system is illustrated in Warn-Varnas *et al.*

Note that the numerical simulations and the laboratory experiments were not performed for identical conditions; several small differences did exist. For the simulations, the change in rotation rate was effectively instantaneous; but, for the experiments, there were small time delays due to the inertia of the turntable. The simulations were carried out with $r_i = 0{\cdot}01$ cm (equation (15)). Warn-Varnas *et al.* showed that an increase of r_i to 0·1 cm made no difference to the results in their investigation.

Figure 1 is a typical set of comparisons of numerical results with LDV measurements for spin-up from rest. The experimental parameters and non-dimensional parameters are given in table 1 under run number N2. The plots show scaled non-dimensional azimuthal velocity $v/r\Omega$ versus non-dimensional time T. Wedemeyer's inviscid solution, (5), and Venezian's solution, (7), are also shown. The radial positions of figure 1 are at (*a*) $r/a = 0{\cdot}75$ and (*b*) $r/a = 0{\cdot}50$. Excellent agreement between the numerical results and the measurements is apparent. Many other comparisons, which are not shown, gave similar agreement. Clearly, the code accurately simulates the flow and the small differences between the numerical model and the experiments do not produce significant differences in the results.

Run number	Radius a (cm)	Height h (cm)	Rotation rate Ω (s^{-1})	Ekman number E	$E^{\frac{1}{2}}(h/a)^2$	τ (s)	$E^{\frac{1}{2}}\Omega^2 a$ (cm s^{-2})
N1	10·14	10·05	0·211	$4{\cdot}36\times10^{-4}$	$2{\cdot}05\times10^{-2}$	227·0	$9{\cdot}4\times10^{-3}$
N2	10·14	10·05	1·002	$9{\cdot}18\times10^{-5}$	$9{\cdot}41\times10^{-3}$	104·2	$9{\cdot}8\times10^{-2}$
N3	10·14	10·05	3·487	$2{\cdot}63\times10^{-5}$	$5{\cdot}04\times10^{-3}$	55·92	$6{\cdot}3\times10^{-1}$
N4	10·14	31·78	1·002	$9{\cdot}18\times10^{-6}$	$2{\cdot}98\times10^{-2}$	329·4	$3{\cdot}1\times10^{-2}$
N5	10·14	3·178	1·002	$9{\cdot}18\times10^{-4}$	$2{\cdot}98\times10^{-3}$	32·94	$3{\cdot}1\times10^{-1}$

TABLE 1. Parameters for numerical calculations, $\nu = 9{\cdot}3\times10^{-3}$ cm^2 s^{-1}

4. The numerical solutions

The results of numerical simulations for four cases of spin-up from rest in a cylinder, which are typical of laboratory experiments, are presented in this section. All the relevant experimental and non-dimensional parameters are listed in table 1. To identify the dynamical processes at work in the vicinity of the front and elsewhere, profiles of selected linear, nonlinear, and viscous terms, as well as the velocity components, were computed.

4.1. *Diagnostic studies and flow fields*

Noting that the dominant flow is in the azimuthal direction and that the azimuthal velocity is vertically uniform in the interior for the small Ekman numbers considered in this paper, diagnostic studies of the terms on the right-hand side of the azimuthal momentum equation (9) were made for one vertical level only ($z/h = -0{\cdot}07$). The first four terms on the right-hand side of (9) are due to the inviscid dynamic effects. They are respectively: radial advection, vertical advection, curvature effect and Coriolis acceleration. The fifth term on the right-hand side of (9) denotes viscous diffusion effects.

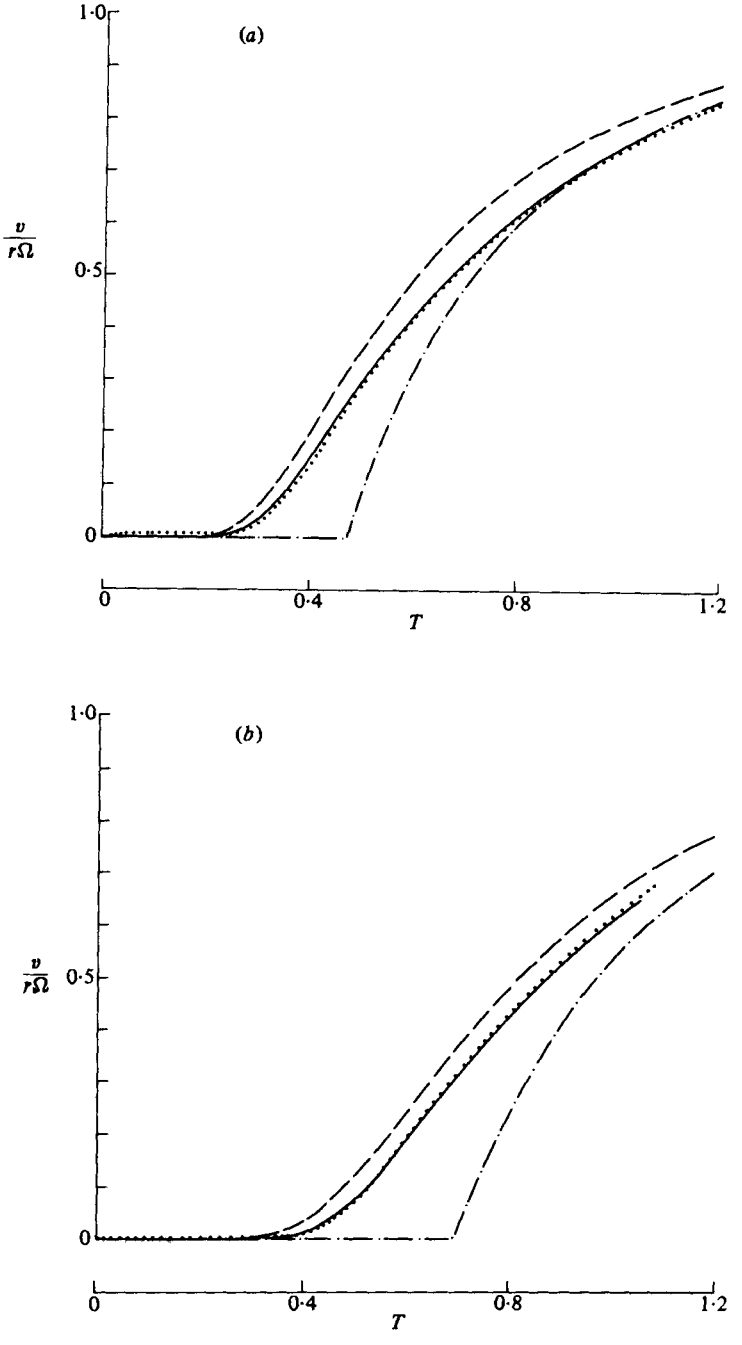

FIGURE 1. Azimuthal velocities for run N2. The ordinate denotes the scaled azimuthal velocity in an inertial frame. The abscissa denotes the scale time $T = t/\tau$. —·—, Wedemeyer's inviscid solution; —, numerical results; ..., LDV measurements; – – –, Venezian's profile. The vertical location is at mid-depth. The radial locations R are (*a*) 0·75; (*b*) 0·5.

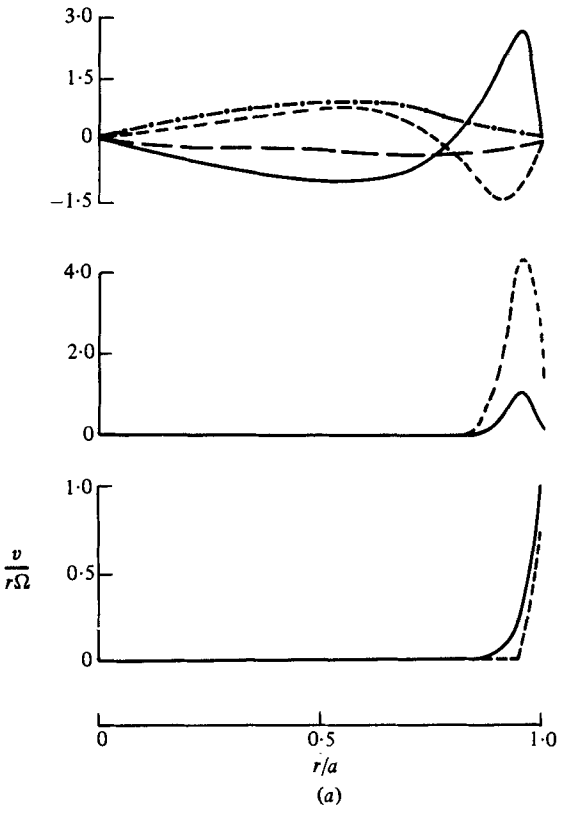

FIGURE 2(*a*). For caption see p. 275.

The results are displayed in figures 2 and 3 as radial profiles for separate times of the individual dynamic effects that make up the azimuthal acceleration, $\partial v'/\partial t$. The values of each term are measured in units of $E^{\frac{1}{2}}a\Omega^2$, which scales the time acceleration $\partial v'/\partial t$. Notice the differences in scale in the ordinates in the figures. In figures 2 and 3 the top plots show the radial profiles of the four individual inviscid terms. Note that the plot of the Coriolis acceleration may also be interpreted as the radial-velocity plot with the factor -2Ω, since to leading order the radial velocity u is also independent of the depth. These Coriolis-acceleration plots are used to determine u in the interior. The middle plots compare the combined inviscid effect, the sum of the preceding four terms, with the viscous-diffusion effect.

In figures 2 and 3 the bottom plots display the radial profile of the scaled non-dimensional azimuthal velocity $v/r\Omega$ in the inertial frame (note that $v = v' + r\Omega$). Wedemeyer's inviscid solution, (4), is also shown. The azimuthal-flow data are included with the diagnostic study plots to reveal the relative phases between the arrival of the front and the changes in the dynamic effects. Figure 4 shows the dynamic effects and flow profiles for larger times when the central core has been substantially spun up. Figures 5 and 6 show the scaled non-dimensional vertical velocity, $w/(\nu\Omega)^{\frac{1}{2}}$, as a function of height for the lower half of the cylinder and for specific times. The radial variation is shown by separate curves on each graph. The results in figure 4 are for the same numerical simulation as the results in figure 2, namely run N1; the results in figures 5 and 6 are for the same simulations as the results in figures 2 and 3, namely runs N1 and N3 respectively (see table 1).

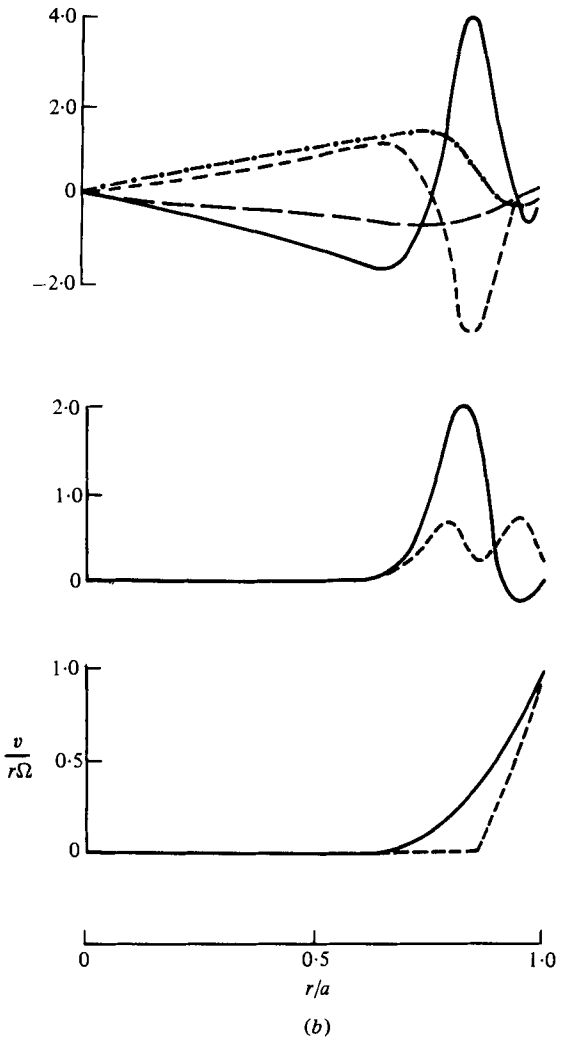

(b)

FIGURE 2(b). For caption see p. 275.

4.2. *General properties of the flow*

Since the spin-up flow is symmetric about the mid-depth plane, $z = 0$, the ensuing discussion is concerned with the flow in the lower half of the cylinder only.

Consider the region far ahead of the front. The azimuthal velocity with respect to the inertial frame is zero, $v' = -r\Omega$; the radial velocity component u is inwards (figures 2 and 3, the top plots); and the vertical velocity component is downwards (figures 5 and 6). Clearly, fluid is sucked into the Ekman layers, and, to satisfy continuity, fluid moves inwards and downwards in the interior. The viscous-diffusion term in (9) is identically zero. The nonlinear advection terms in (9) reduce to

$$-\frac{1}{r}\frac{\partial}{\partial r}(ruv') = r\Omega\left(\frac{\partial u}{\partial r} + \frac{2u}{r}\right), \tag{16}$$

$$-\frac{\partial}{\partial z}(v'w) = r\Omega\frac{\partial w}{\partial r}. \tag{17}$$

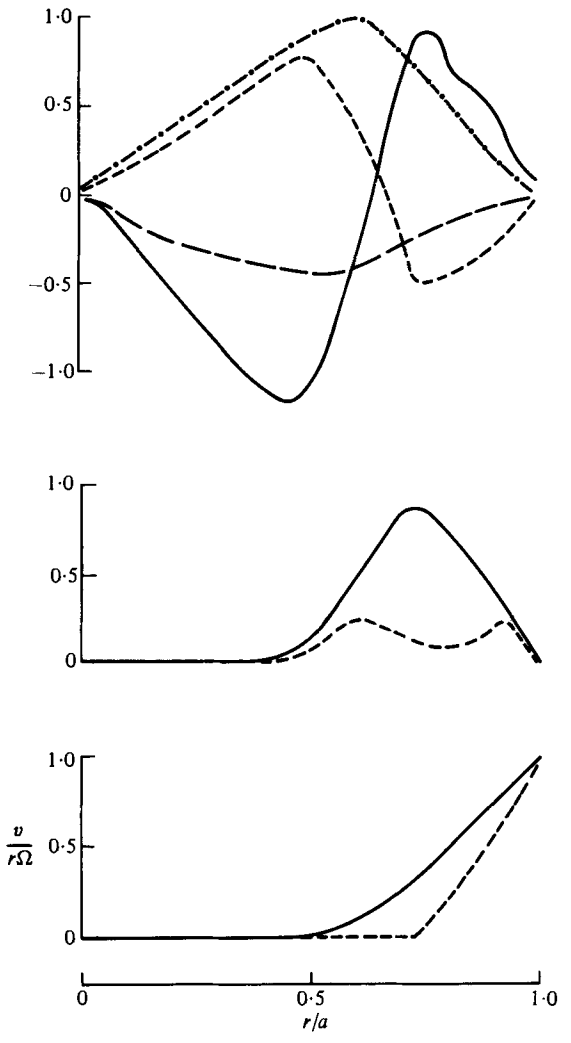

(*c*)

FIGURE 2(*c*). For caption see p. 275.

Since $u = 0$ on the symmetry axis and since u has a maximum negative value in the interior, (16) indicates that the radial-advection term should be negative. Since at mid-depth $w = 0$ because of symmetry and, consequently, $\partial w/\partial z > 0$, (17) indicates that the vertical-advection term should be positive. The curvature term $-v'u/r$ should be negative. The results in the top plots of figures 2 and 3 are consistent with these conclusions. The inviscid terms add up to zero; so there is no spin-up ahead of the front. The vertical velocity w is independent of the radial location, indicating a uniform Ekman suction (see curves (*a*) and (*b*) of figure 5). In the interior, a linear dependence of w on z is apparent, and the edge of the Ekman layer where the suction is greatest ($w = \tilde{w}_\infty$, see §3) can be easily identified.

As the fluid begins to spin up upon the arrival of the front, the flow field changes, and some of the terms undergo rapid variations. The inwards radial velocity $-u$ approaches a maximum value and then decreases, while w goes to zero and then becomes upwards. The middle plots of figure 2, for intermediate times when the front

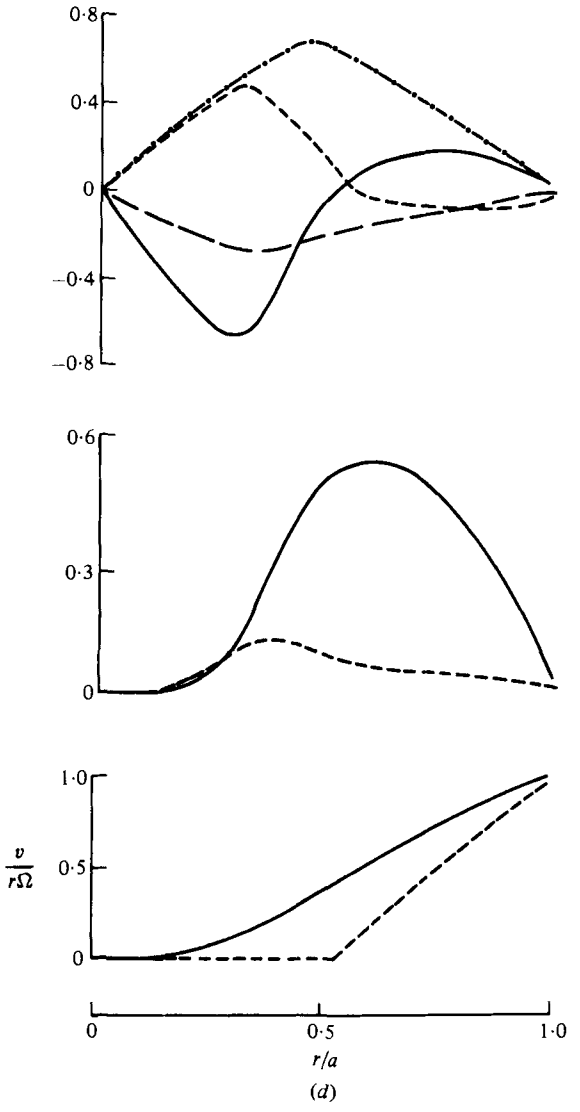

FIGURE 2(*d*). For caption see facing page.

has propagated into the interior, show that the viscous-diffusion term increases from zero, reaches a maximum, and then decreases (e.g. figure 2(*c*)). This region of enhanced viscous activity reveals the thickness of the front. Inspection of the viscous-diffusion plots gives the thickness $O(E^{\frac{1}{4}}h)$, which is consistent with the analytical result of Venezian (see §2.2). Changes in the advection terms across the front are also noticeable. The value of the radial advection term changes from a negative minimum at the leading edge of the front to a positive maximum at the trailing edge. A similar observation, but with reversed signs, can be made for the radial profile of the vertical-advection term.

Finally, consider the region between the front and the sidewall. Again, the radial velocity is inwards and decreases to zero at the sidewall, and w is upwards. Figure 2(*a*) shows that, for very early times, the viscous-diffusion term is strong in a single region close to the sidewall. For intermediate times, figures 2 and 3 show that the

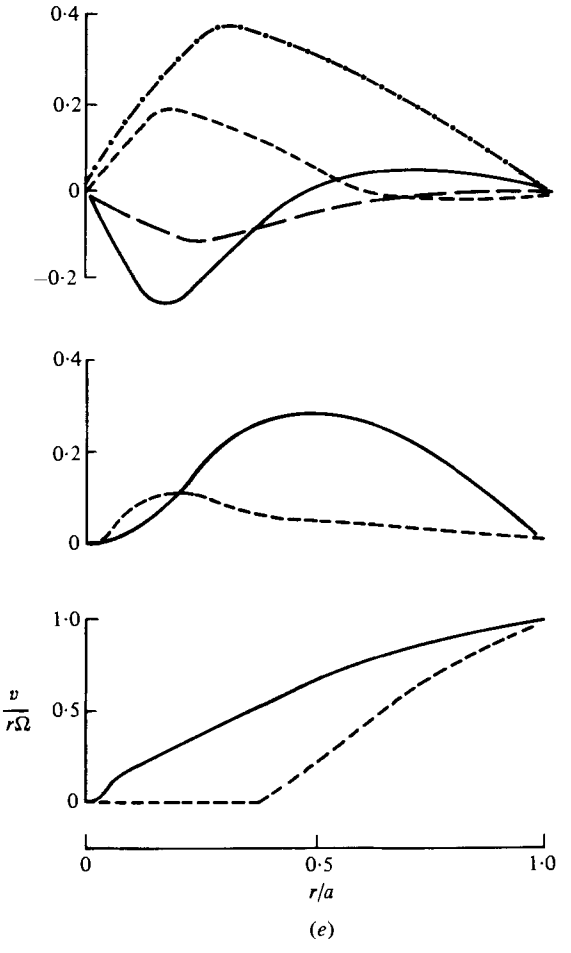

FIGURE 2. The top and middle plots show the radial profiles near mid-depth of each term on the right-hand side of (2) for run N1. In the top plot: —; radial advection; ----, vertical advection; —·—, Coriolis acceleration; – –, curvature effect. In the middle plot: —, the sum of the above four terms; ----, the viscous-diffusion term. The ordinates of the top and the middle plots are in units of $E^{\frac{1}{2}}\Omega^2 a$. In the bottom plot: —, the numerical results; ----, Wedemeyer's inviscid solution. The ordinate of the bottom plot denotes the scaled azimuthal velocity on the inertial frame. Times T are (*a*) 0·053; (*b*) 0·158; (*c*) 0·317; (*d*) 0·634; (*e*) 0·952.

viscous term reaches a minimum behind the front and then increases again close to the sidewall (see figures 2*b*, *c*). This indicates the presence of a viscous boundary layer on the sidewall. For later times, when the fluid near the sidewall is almost completely spun up, this sidewall layer vanishes (see figures 2*d*, *e*). The magnitude of w behind the front increases with r until the sidewall boundary layer is reached, over which w decreases to zero on the sidewall. In general, w in the interior region behind the front is less linear in z than in the region ahead of the front. The preceding results are consistent with the following picture of the evolving flow given by Benton & Clark (1974). Strong nonlinearity causes the $E^{\frac{1}{4}}$ layer of linear theory to break away from the wall and propagate into the interior as the moving front; an $E^{\frac{1}{3}}$ layer remains behind to reduce the vertical velocity to zero.

In general, behind the front both the radial advection and vertical advection vary

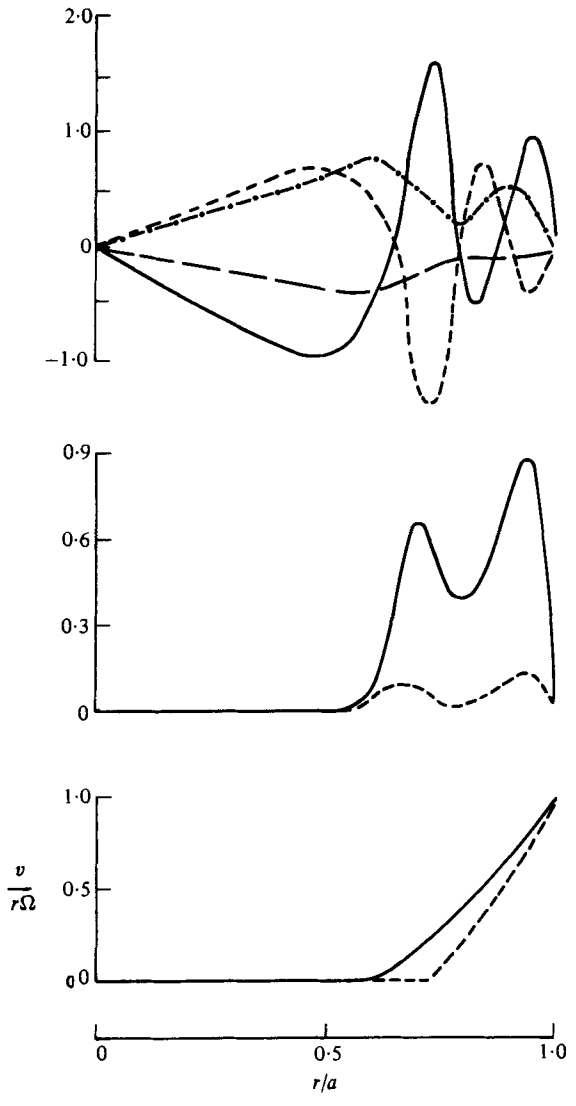

FIGURE 3. Same as in figure 2, but for run N3 at $T = 0{\cdot}321$.

monotonically to zero on the sidewall. However, in figure 3 the radial advection and the vertical advection undergo rapid changes in early times close to the sidewall. This point will be further discussed in §4.3.

Throughout the spin-up motion, figures 2 and 3 show that the Coriolis acceleration $-2\Omega u$ increases from zero on the axis to a maximum in or near the frontal region and then decreases to zero at the sidewall; while the curvature term $-vu/r$ decreases from zero on the axis to a minimum in or near the frontal region and then decreases to zero on the sidewall. Figures 5 and 6 show that w is very small in the frontal region. These results imply that the meridional flow within the front is predominantly in the radial direction. Note also that, for intermediate times, in the region between the front and the sidewall, the combined dynamic effects still produce a relatively large positive value of the fluid acceleration. This indicates that spin-up is continuing in

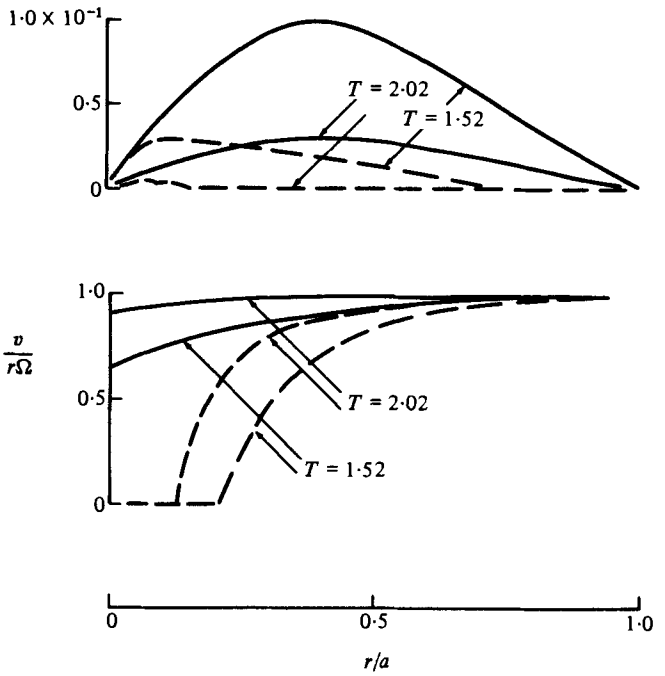

FIGURE 4. Flow behaviour of run N1 at large times. In the top plot: —, the sum of the inviscid terms; ----, the viscous-diffusion term. The ordinate of the top plot is in units of $E^{\frac{1}{2}}\Omega^2 a$. The bottom plot shows the scaled azimuthal velocity: —, numerical results; ----, Wedemeyer's inviscid solution.

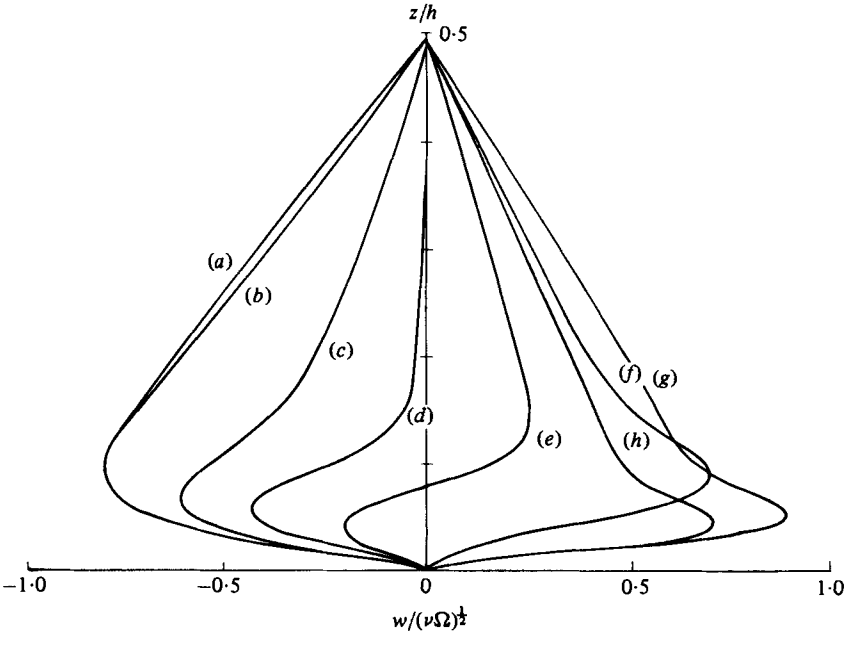

FIGURE 5. Plots of the vertical velocity w for run N1 at $T = 0{\cdot}317$. The radial locations R of the curves are (*a*) 0·33; (*b*) 0·40; (*c*) 0·60; (*d*) 0·65; (*e*) 0·70; (*f*) 0·80; (*g*) 0·925; (*h*) 0·975.

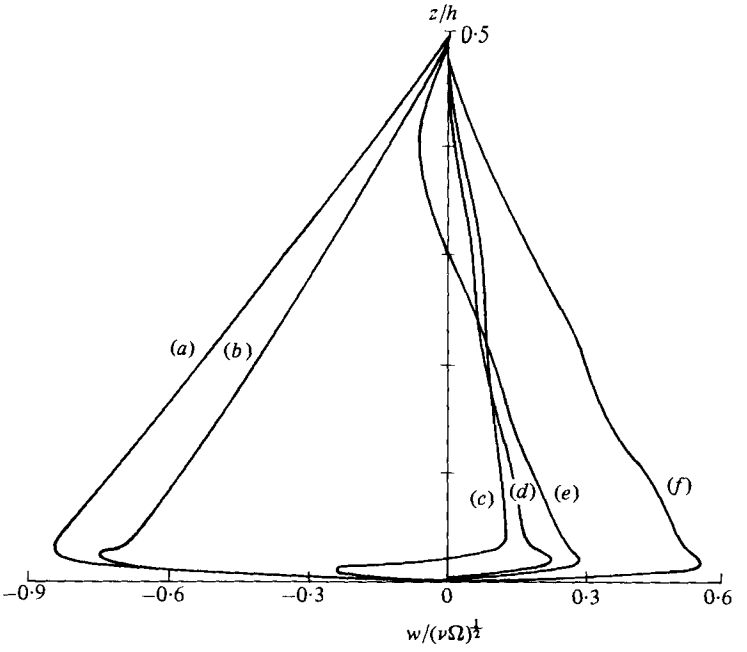

FIGURE 6. Plots of the vertical velocity w for run N3 at $T = 0{\cdot}545$. The radial locations R of the curves are (*a*) 0·4; (*b*) 0·5; (*c*) 0·6; (*d*) 0·7; (*e*) 0·8; (*f*) 0·9.

this region. In general, the azimuthal acceleration has its maximum value just to the rear of the front.

Figure 2 shows the changes in the relative contributions of the different terms to the spin-up process over the time interval τ. Immediately after the impulsive start, viscous diffusion near the sidewall is the major contributor to spin-up, then the nonlinear radial advection term takes over. Eventually for $T \gtrsim 0{\cdot}5$, as the flow gradients weaken, the linear Coriolis force dominates.

Figure 2(*e*) shows that, even after $T \approx 1$, the central core of fluid near the axis is only slightly spun up. To investigate further the spin-up process in this region, run N1 was extended to longer times. Figure 4 shows that for $T = 2{\cdot}02$, $v/r\Omega \gtrsim 0{\cdot}9$, and the central core is substantially spun up. Further, at this time, the Coriolis force still dominates the spin-up process; viscous effects are small, which is what we expect since the fluid is close to solid-body rotation.

4.3. *Effects of the experimental parameters*

The non-dimensional Ekman-layer thicknesses ($\delta/h = E^{\frac{1}{2}}$) for runs N1 and N3 are 0·021 and 0·0096 respectively. These different thicknesses are clearly revealed by comparing figures 5 and 6. A similar comparison was attempted for the thicknesses of the propagating front and the stationary sidewall layer, as revealed by the viscous-diffusion terms in the middle plots of figures 2 and 3. The impression gained is that, unlike the Ekman layer, the propagating front thickens with time, but the sidewall layer maintains a constant thickness (see figures 2*b–d*). No obvious difference in the frontal thickness is apparent between the two runs, but this is hardly surprising since $E^{\frac{1}{4}}$ does not vary by much. To study these boundary-layer thicknesses further, data with more resolution in space and time are required.

Watkins & Hussey (1977) suggested that $A^{-2}E^{\frac{1}{2}}$ is a more relevant parameter for

the spin-up flow than E. Runs N4 and N5 were performed for different selected cylinder depths, so that comparison could be made for similar values of $A^{-2}E^{\frac{1}{2}}$ and different values of E (see table 1). Such comparisons between the results of N1 and N4 and the results of N3 and N5 for similar values of T and $A^{-2}E^{\frac{1}{2}}$, which are not shown in this paper, are in strong agreement with the suggestion.

In figure 3 the radial and vertical advection terms undergo rapid change close to the sidewall. The variations of the advection terms are similar to their variations across the front. These results, observed when strong inertial effects are present ($A^{-2}E^{\frac{1}{2}} \ll 1$), are almost certainly related to the regions of reversed flow and inertial waves found by Kitchens (1980) for similar times, locations, and parameters (see §2.3).

We now define the arrival time of the front (non-dimensionalized by τ), T_{f} as the time for the azimuthal velocity v to reach $0{\cdot}05r\Omega$, and a spin-up time (similarly non-dimensionalized) T_{h} as the time for v to reach $0{\cdot}5r\Omega$. In figure 7, we plot T_{f} and T_{h} as functions of $A^{-2}E^{\frac{1}{2}}$ for the experiments listed in table 1. Two radial positions $R = 0{\cdot}788$ and $0{\cdot}388$ are considered. Also plotted in figure 7 are available data from Watkins & Hussey (1977), Wedemeyer's inviscid solution, (4), and measurements of Weidman (1976*b*) for nearly impulsive spin-up from rest.

Figure 7 reveals a systematic dependence of T_{f} and T_{h} on $A^{-2}E^{\frac{1}{2}}$ for the results from our numerical model. (Table 1 shows no such dependence on E.) The values of T_{h} from the measurements of Watkins & Hussey show values consistent with our results. However, the values of T_{h} from the computations by Watkins & Hussey based on Wedemeyer's viscous equation, (3), are not in such good agreement with our results. The predictions of Wedemeyer's solution also show discrepancies. Weidman's data were interpolated to give values of T_{f} and T_{h} for $R = 0{\cdot}388$ and $0{\cdot}788$. For $R = 0{\cdot}788$ the agreement is good, but for $R = 0{\cdot}388$ it is poor. In his experiments Weidman observed turbulent flow near the sidewall at the early stages of spin-up. This is not surprising since he used a large value of Ω ($= 108{\cdot}7\ \mathrm{s}^{-1}$). The faster times for $R = 0{\cdot}788$ are almost certainly due to the turbulence. We conclude that $A^{-2}E^{\frac{1}{2}}$ is a good parameter for collapsing data for the spin-up flow.

5. Conclusions

The impulsive spin-up from rest of a homogeneous fluid in a cylinder for small Ekman numbers has been investigated numerically. The numerical simulations employed finite-difference techniques on the Navier–Stokes equations in axisymmetric form. The numerical model was thoroughly checked by comparing its predictions against accurate measurements of the azimuthal flow for spin-up from rest, made with a rotating laser-Doppler velocimeter. Excellent agreement was obtained.

New, three-dimensional flow-field data from a range of Ekman numbers $9{\cdot}18 \times 10^{-6} \leqslant E \leqslant 9{\cdot}18 \times 10^{-4}$ are presented. The data enable us to fill in the details of the azimuthal and meridional flows not accurately given by the Wedemeyer model and its extensions. Diagnostic studies of the azimuthal momentum equation in the interior were made. These studies show the contributions to spin-up of the separate inviscid and viscous terms as a function of radius and time. The moving shear-discontinuity front of Wedemeyer's inviscid solution is shown to be a propagating layer of enhanced local viscous activity. The thickness of the front is seen to be consistent with Venezian's (1970) analysis. Ahead of the front, both the combined inviscid dynamic effect and the viscous-diffusion effect are zero; there is no spin-up until the arrival of the front. Across the front some of the terms undergo rapid

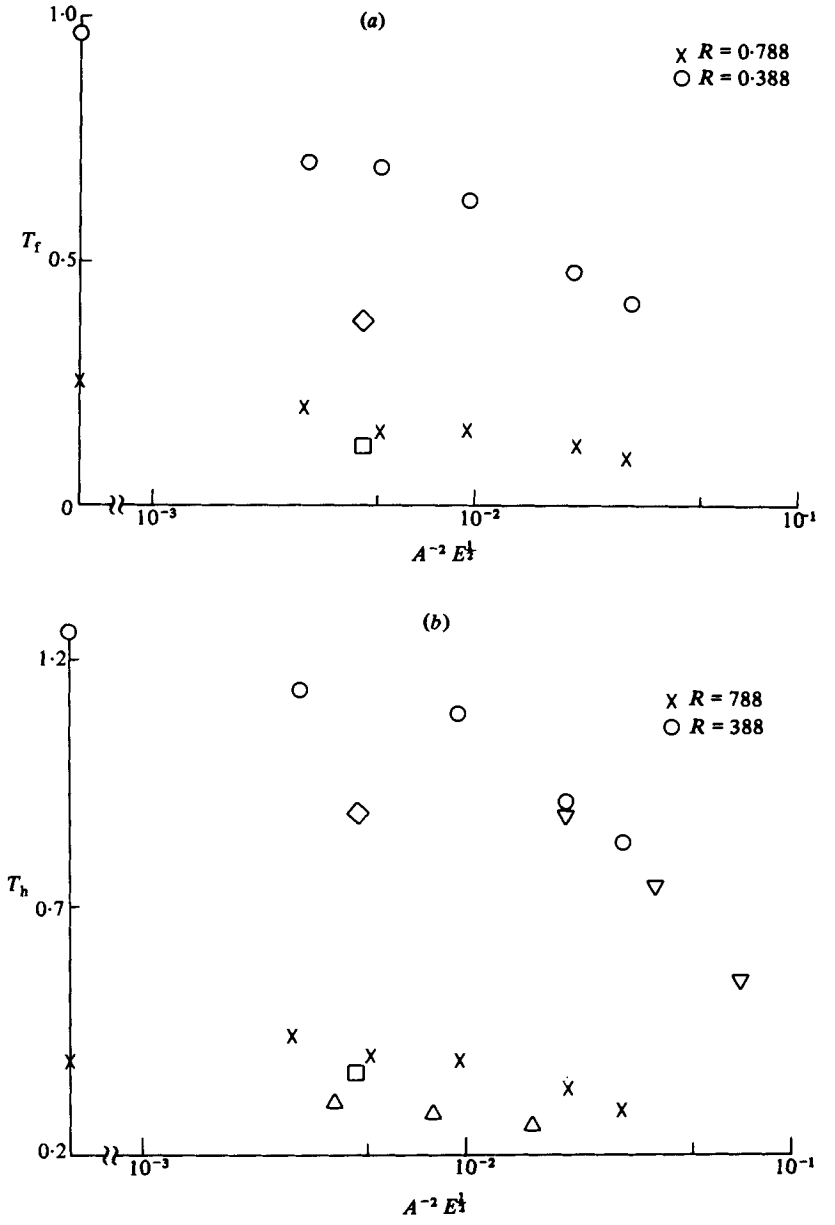

FIGURE 7. Plots of the non-dimensional arrival time of the front T_f shown in (*a*), and the half-time T_h shown in (*b*), as functiomns of $A^{-2}E^{\frac{1}{2}}$. Wedemeyer's inviscid solutions, (4), are shown on the ordinate. In (*b*), ∇ denotes the experimental data of Watkins & Hussey at $R = 0{\cdot}395$, and $\triangle$ denotes the results of their computations of Wedemeyer's viscous equation, (3), at $R = 0{\cdot}805$. The measurements by Weidman are shown by $\diamond$ for $R = 0{\cdot}388$ and $\square$ for $R = 0{\cdot}788$.

variations. In general, the azimuthal acceleration has its maximum value just to the rear of the front. Behind the front, the terms vary less rapidly; the viscous effect decreases but then increases again in the sidewall boundary layer.

Immediately after the impulsive start, before the Ekman layers have had a chance to form, viscous diffusion at the sidewall is the major contributor to spin-up. Then, when the Ekman flux is established, the nonlinear radial advection term takes over.

As spin-up progresses, the strength of the nonlinearity and consequently the strength of the front diminish. At large times, the linear Coriolis acceleration becomes the dominant term.

In the interior, the meridional circulation is everywhere radially inwards. Ekman suction causes the fluid ahead of the front to be drawn into the Ekman layer and the fluid behind the front to be blown out of the Ekman layer. At the core of the front, the magnitude of the inwards radial flow is a maximum, and the vertical velocity is very small. Strong radial gradients of vertical velocity are observed everywhere at the edge of the Ekman layer, except far ahead of the front, and the azimuthal flow behind the front shows strong departures from solid-body rotation.

These results show that the Wedemeyer model describes the flow accurately in the region ahead of the front. However, in the vicinity of the front and behind the front, the assumptions made by Wedemeyer are not accurate and his model is less quantitative.

We wish to acknowledge the referees' comments which led to improvements in the paper. J.M.H. is indebted to the National Research Council for a Senior Research Associateship and to the USRA for a Visiting Scientist appointment which were held consecutively during the performance of this investigation. These appointments and the research were supported by the Global Weather Program of the Office of Space Science and Applications, NASA Headquarters, Washington, D.C.

REFERENCES

BENTON, E. R. 1979 Vorticity dynamics in spin-up from rest. *Phys. Fluids* **22**, 1250.

BENTON, E. R. & CLARK, A. 1974 Spin-up. *Ann. Rev. Fluid Mech.* **6**, 257.

GREENSPAN, H. P. 1968 *The Theory of Rotating Fluids.* Cambridge University Press.

GREENSPAN, H. P. & HOWARD, L. N. 1963 On a time-dependent motion of a rotating fluid. *J. Fluid Mech.* **17**, 385.

HYUN, J. M., FOWLIS, W. W. & WARN-VARNAS, A. 1982 Numerical solutions for the spin-up of a stratified fluid. *J. Fluid Mech.* **117**, 71.

KITCHENS, C. W. 1979 Navier–Stokes solutions for spin-up from rest in a cylindrical container. *ARBRL-TR-02193, Ballistic Research Laboratory, Aberdeen Proving Ground, Maryland.*

KITCHENS, C. W. 1980 Navier–Stokes solutions for spin-up in a filled cylinder. *A.I.A.A. J.* **18**, 929.

ROGERS, M. H. & LANCE, G. N. 1960 The rotationally symmetric flow of a viscous fluid in the presence of an infinite rotating disk. *J. Fluid Mech.* **7**, 617.

VENEZIAN, G. 1969 Spin-up of a contained fluid. *Topics in Ocean Engng* **1**, 212.

VENEZIAN, G. 1970 Nonlinear spin-up. *Topics in Ocean Engng* **2**, 87.

WATKINS, W. B. & HUSSEY, R. G. 1973 Spin-up from rest: limitations of the Wedemeyer model. *Phys. Fluids* **16**, 1530.

WATKINS, W. B. & HUSSEY, R. G. 1977 Spin-up from rest in a cylinder. *Phys. Fluids* **20**, 1596.

WARN-VARNAS, A., FOWLIS, W. W., PIACSEK, S. & LEE, S. M. 1978 Numerical solutions and laser-Doppler measurements of spin-up. *J. Fluid Mech.* **85**, 609.

WEDEMEYER, E. H. 1964 The unsteady flow within a spinning cylinder. *J. Fluid Mech.* **20**, 383.

WEIDMAN, P. D. 1976*a* On the spin-up and spin-down of a rotating fluid. Part 1. Extending the Wedemeyer model. *J. Fluid Mech.* **77**, 685.

WEIDMAN, P. D. 1976*b* On the spin-up and spin-down of a rotating fluid. Part 2. Measurements and stability. *J. Fluid Mech.* **77**, 709.